Underwater LED-based Lagrangian Particle Tracking Velocimetry

Ignazio Maria Viola[1,*], Alex Nila[2], Tom Davey[1] and Roman Gabl[1]

[1] School of Engineering, Institute for Energy Systems, University of Edinburgh, EH9 3BF, U.K.
E-mails: i.m.viola@ed.ac.uk, tom.davey@flowave.ed.ac.uk, roman.gabl@ed.ac.uk
web: https://voilab.eng.ed.ac.uk; https://flowave.eng.ed.ac.uk

[2] Lavision U.K. Ltd., Bicester, EH8 9AB, U.K.
E-mail: anila@lavision.com, web: http://www.lavision.co.uk

[*] Corresponding author: Ignazio Maria Viola, i.m.viola@ed.ac.uk

ABSTRACT

We present a new white-light volumetric flow measurement technique that can be used in large-scale facilities. The technique enables measuring a volume that is two orders of magnitude higher than stereo PIV, with a comparable time and space resolution and without the need for a class-4 laser. We demonstrate this LED-based Lagrangian particle tracking velocimetry by measuring the tip vortex formation and the near wake of a 1.2 m diameter tidal turbine in a 25 m diameter, 2 m deep tank. We combine together 7 streamwise-distributed volumes of interests, each 300 mm long, 200 mm wide and 100 mm deep, reaching up to one diameter downstream of the turbine. The system does not require re-calibration when moved. By assuming a periodic flow field, we reconstructed a phased-averaged flow field with a time resolution of 3.9 ms and a space resolution of 5.4 mm. This novel methodology can enable a step change in the flow diagnostic capabilities of large scale marine facilities. The large volume and comparatively high time and space resolution could enable addressing key research questions on high-Reynolds-number flows and could provide valuable benchmark data for numerical model development and code validation.

Keywords: Lagrangian particle tracking velocimetry; flow diagnostics; LED illumination; tidal turbine hydrodynamics; tip vortex; rotor wake.

NOMENCLATURE

D	Rotor diameter [m]
U	Mean free stream velocity [m s^{-1}]
U_v	Mean convection velocity of the tip vortices [m s^{-1}]
$\mathbf{u} = (u, v, w)$	Flow velocity [m s^{-1},m s^{-1},m s^{-1}]
(x, y, z)	Cartesian coordinates [m,m,m]
λ_2	Swirling strength [s^{-2}]
κ	Turbulent kinetic energy [m^2 s^{-2}]
$\boldsymbol{\omega} = (\omega_x, \omega_y, \omega_z)$	Vorticity vector [s^{-1},s^{-1},s^{-1}]
$\langle\cdot\rangle$	Phase-average operator
$\bar{\cdot}$	Time-average operator
LED	Light-emitting diode
OTF	Optical transfer function
PIV	Particle image velocimetry
RPM	Revolution per minute
STB	Shake the Box
VOI	Volume of interest
VSC	Volume self calibration

1 INTRODUCTION

Tidal energy is a promising renewable energy source that could critically contribute to energy security in several countries including the United Kingdom and the European Union, which have highly energetic tidal sites. The world's first arrays of tidal turbines (Meygen and Nova's Bluemull Sound) have just recently been deployed in Scotland and research will need to support industry development by understanding the complex wakes of these devices. Yet, the characterisation of tidal turbine's wakes remains very challenging both experimentally and numerically (Day *et al.*, 2015; Adcock *et al.*, 2021).

Due to the anisotropy of the wake and its wide range of temporal scales, experimental measurements are needed to inform numerical simulations on appropriate models (Afgan *et al.*, 2013; Tedds *et al.*, 2014; Lloyd *et al.*, 2014; Olczak *et al.*, 2016; Ahmed *et al.*, 2017; Ouro & Stoesser, 2019). The anisotropy of the wake turbulence does not only derives from the tip vortices and the global flow rotation around the turbine axis (Chamorro *et al.*, 2013; Chen *et al.*, 2017), but also because of the seabed and free-surface blockage that accelerates the bypass flow more than on the sides of the turbines (Tedds *et al.*, 2014; Stallard *et al.*, 2013, 2015; Chen *et al.*, 2017). In this paper, we will demonstrate a white-light Lagrangian particle tracking velocimetry and show how it can contribute to tackle some of these outstanding research questions.

Compared to, for instance, ship propellers (Felli *et al.*, 2011), tidal turbine models need to be comparatively larger to ensure mild Reynolds number effects. For example, turbine models that are of the order of 1 m in diameter with a blade chord of 0.1 m can be tested in a 1 m s^{-1} current. At typical tip speed ratios around five (Gaurier *et al.*, 2013), the chord-based Reynolds number varies from 10^5 at the root to more than 5×10^5 at the tip. Decreasing the Reynolds number by more than an order of magnitude from these values, the thrust would show a non-realistic step change due to laminar separation on the blades (Luznik *et al.*, 2013). Hence, tidal turbine wakes are often investigated in large scale facilities with test sections that can accommodate a metre-scale rotor (Gaurier *et al.*, 2013; Milne *et al.*, 2015; Lust *et al.*, 2015; Payne *et al.*, 2017).

A key challenge of testing in larger facilities is that these are not always compatible with laser-based flow diagnostics (Adrian *et al.*, 2011; Raffel *et al.*, 2018). Space and time resolved flow measurement that is capable to resolve the dynamics of the tip vortices in the wake typically requires a class 4 laser illumination (Fontaine *et al.*, 2014; Lust *et al.*, 2015; Shi *et al.*, 2017; Nuernberg & Tao, 2018; Gaurier *et al.*, 2020). Class 4 lasers are highly dangerous because they can damage the eye and the skin causing blindness and burns, and they can cause fires. To ensure safe use of these lasers, the light is often enclosed preventing accidental exposure trough a physical barrage, which is not practical in large scale facilities. In this paper we demonstrate a first of its kind experimental apparatus that allows undertaking accurate flow visualisation with only harmless white light illumination.

Eye-safe Light-Emitting Diode (LED) illumination for Particle Image Velocimetry (PIV) measurements has been demonstrated for large-scale flow measurements in air (Usherwood *et al.*, 2020; Schanz *et al.*, 2018). In contrast, here we present one of the first applications of LED illumination for large-scale flow measurements in water. In Roettig *et al.* (2019), the use of an underwater volumetric flow measurement approach is presented, with mainly a fibre-delivered laser illumination being used. In the same work, the authors present the potential of LED-based illumination for one of the test cases studied, with promising results. However, to the best of the authors' knowledge, no in-depth work has been published using LED-based illumination underwater for volumetric full-field flow measurements.

The rest of the paper is organised as follows. In §2 (Experimental Conditions) we present the facility (§2.1) and the turbine (§2.2) used for this demonstration. The flow conditions measured in the absence of the turbine are presented in §2.3. In §3 (Lagrangian Particle Tracking Velocimetry), the new system is presented in detail, including the hardware (§3.1), the calibration (§3.2) and the general data processing associated with the technique (§3.3). In §4 (Example of Application), we present an example of results and the specific data processing associated with these results. This section is broken down into the visualisation of the formation of the tip vortices (§4.1) and of the overall flow in the

near wake (§4.2). A discussion on the main results is included in §5 (Discussion and Conclusions).

2 EXPERIMENTAL CONDITION

2.1 Facility

Testing was conducted in the FloWave Ocean Energy Research Facility of the University of Edinburgh, Scotland (Figure 1). FloWave is a 25 m diameter and 2 m deep tank for testing offshore wave and current energy harvesters in combined wave and current conditions. An array of 168 wave paddles along the perimeter of the tank allow waves to be generated in multiple directions, including monochromatic waves and random seas. This study, however, was undertaken in current only and nominally flat water without actuation of the wave paddles. Current can also be generated in any direction. The flow is recirculated through turning vanes under the wave paddles through a chamber under the main test volume. The lower chamber is equipped with 28 propellers around the perimeter. By controlling individually the velocity of each propeller, it is possible to generate currents in excess of 1.6 m s^{-1} in any direction. The specific current conditions during the test are presented in §2.3.

Figure 1. The 25-m-diameter circular facility FloWave at the University of Edinburgh.

2.2 Turbine

Figure 2 shows an underwater picture of the axial in-stream turbine. The diameter of the rotor is $D = 1.2$ m, and the diameter of the hemispherical hub is $0.1D$. The rotor axis is at 1 m from the floor, i.e. vertically centred with respect to still water depth. The nacelle is a torpedo $0.86D$ long, including the hub and the downstream hemispherical cap. It extends beyond the tower with a larger diameter of $0.13D$. The axis of the cylindrical tower is $0.4D$ downstream of the rotor plane and has a diameter of $0.085D$. The turbine aims to represent a realistic megawatt turbine at a 1:15 scale. More details on its design can be found in Payne *et al.* (2017).

The turbine is equipped with three blades, whose geometry is available at `https://datashare.is.ed.ac.uk/handle/10283/2356`. The blade pitch was kept constant at the design value.

The angular velocity of the turbine was controlled with an incremental quadrature encoder, delivering a resolution of 16384 (14-bit) pulses per revolution. Contemporaneous angular velocity data was not available. A later repeat test of the turbine under the same ambient conditions showed a mean velocity of 88.9 Revolutions Per Minute (RPM) and a standard deviation of 1.31 RPM, equivalent to a tip speed ratio of seven.

Whilst the turbine can be equipped with sensors to measure torque, thrust, and root bending moment

of each blade, these were not available at the time of the test. However, the same turbine was tested in the same flow conditions on other occasions and results from these sensors can be found in Noble *et al.* (2020). For a nominal inflow velocity of 0.8 m s^{-1}, Draycott *et al.* (2019) have measured the power and thrust coefficients of this turbine as approximately 0.42 and 0.72 respectively.

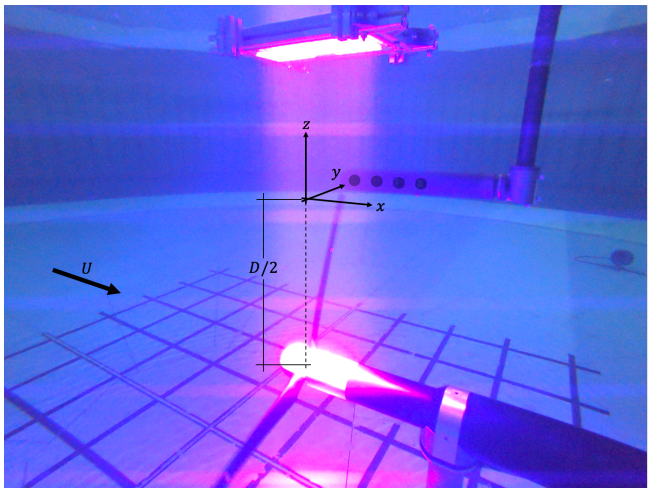

Figure 2. Underwater picture of the tidal turbine illuminated by the LED unit placed above the hub into a container piercing the free surface, and the four streamwise-aligned circular cameras of the shake-the-box system in the background.

2.3 Coordinate System and Free Stream Velocity

The reference system, which is pictured in Fig. 2, is placed on the top of the rotor disk, where the x and z axes are streamwise, and vertical, respectively. The reference systems is centred on the tip of the blade, when this is vertically pointing upwards, within an accuracy smaller than ± 3 mm.

The free stream velocity was measured with an acoustic Doppler velocimeter (Nortek Vectrino Profiler operating in point measurement mode). This velocimeter measures three velocity components at 100 Hz with an accuracy of 1%. The current was characterised by repeating the tests in the absence of the turbine and any other underwater installation. The probe was located at 405 mm (± 1 mm) under the still water level.

The mean and root mean square of the three streamwise velocity components are presented in Table 1. The resolved turbulence intensity was calculated as 6.1%. It is observed that the velocity fluctuations are similar in all axes. While only a point measurement was taken, interested readers can find a description of the spacial variation of the flow field in FloWave in Noble *et al.* (2015). In the following, the mean streamwise velocity $U = 0.866$ m s^{-1} is used to non dimensionalise the results.

Table 1. Flow conditions at $\mathbf{x} = (0, 0, -0.005 \pm 0.001$ m).

Velocity component	**Mean** [m s^{-1}]	**Root mean square** [m s^{-1}]
Streamwise (x)	0.866	0.0615
Crossflow horizontal (y)	0.0139	0.0650
Vertical (z)	-0.00715	0.0531

3 LAGRANGIAN PARTICLE TRACKING VELOCIMETRY

The measurement system used in this study is an underwater flow measurement system making use of LED illumination and an integrated four-camera system. The data processing is done using the state-of-the-art 4D Lagrangian Particle Tracking algorithm, LaVision's Shake-The-Box (STB) module. Data capture, data analysis and post-processing as well as data visualization is performed using DaVis 10 software.

3.1 Hardware

For the measurements presented in this paper, a MiniShaker underwater system is used. The MiniShaker underwater module comprises four cameras, each having a sensor resolution of 896 pixels $\times$ 656 pixels, that can acquire 8 or 10 bit images at a maximum of 510 frames per second, at full resolution. For this study, 8 bit camera images are acquired at 256 frames per second. The cameras are equipped with 7.8 mm focal length lenses, to achieve a maximum Volume of Interest (VOI) of 300 mm $\times$ 220-mm $\times$ 150 mm. The module is enclosed in a watertight stainless steel camera housing and is pre-aligned to be used at a fixed working distance of 600 mm away from the focal plane. This configuration required a single perspective calibration to be performed at the start of the measurement campaign.

The illumination used in this study is achieved using an eye-safe LED Flashlight 300 unit from LaVision. The unit comprises 72 high-powered LEDs which are configured in an array covering an active area of 300 mm $\times$ 100 mm. The light set were enclosed in a transparent, rigid, cuboid container piercing the water. This allowed the lights to underwater while remaining dry and accessible from above water. The lights were triggered with a frequency of 256 Hz, synchronised with the MiniShaker camera module. To achieve the maximum possible level of light intensity, the LED unit is used in a pulsed-overdrive mode, with a 10% duty cycle, and a pulse illumination time of 100 μs.

The MiniShaker camera module and the LED Flashlight 300 are controlled from a Windows 10 PC, using LaVision's DaVis 10 software for data acquisition and analysis, and a programmable timing unit. The time-resolved data is recorded at 256 Hz and stored directly to the PC. The Minishaker and LED box are rigidly mounted to the instrumentation gantry, which allows the system to be translated for later stitching the data in an enlarged VOI. The tracer particles used for these measurements were existing seeding particles present in the water, which are 10 μm hollow-glass particles.

3.2 Calibration

The image data from the four cameras of the MiniShaker module acquired using the DaVis 10 platform, are subsequently analysed using the Shake-The-Box (STB) module of the same software platform. STB is a 4D-Lagrangian particle tracking technique that identifies 3D particle positions and tracks each particle over time (Schanz *et al.*, 2016). The starting point of the analysis is the perspective calibration of the camera system, which allows for algorithm to reconstruct 3D particle positions by triangulating the 2D camera images. For the perspective calibration, a known target needs to be used, with markers present in at least two separate planes in the out-of-plane direction, which, for the reference system in Fig. 2, is the y-direction. In this study, a 300 mm $\times$ 300 mm calibration two-level calibration plate was imaged at three positions along y-direction, namely -70 mm, 0 and 70 mm with respect to the mid-plane of the measurement volume.

The second step of the calibration process consists of a Volume Self-Calibration (VSC) procedure (Wieneke, 2008). During this second step, the mapping function obtained during the first step is refined using particle images of tracer particles within the flow, as imaged by all the cameras in the system at the same instance in time. VSC was applied iteratively to approximately 500 images, by dividing the VOI in $5 \times 5 \times 3$ sub-volumes corresponding to a total physical domain of 300 mm $\times$

220 mm × 140 mm. The total average disparity obtained after the VSC process is lower than 0.1 voxel, corresponding to a valid calibration for volumetric flow measurements (Elsinga *et al.*, 2006).

Finally, the last step in the calibration process is the calculation of an Optical Transfer Function (OTF) (Schanz *et al.*, 2016). As STB is based on diffraction-limited imaging, the particle image shape is directly influenced by the diffraction spot of the lens aperture and the position of the 3D particle relative to the focal plane. To accurately determine the particle image for a certain position in the VOI, an average particle image is calculated for each sub-volume as created in the VSC step and used as the basis for the calculation of the OTF which will be subsequently used in the STB processing.

3.3 Data Processing

Before the STB analysis is undertaken, image pre-processing is performed on the raw data, using a combination of spatial filters. A local sliding minimum intensity value is first subtracted using a kernel of 7 pixels × 7 pixels, to reduce image noise. Secondly, a spatial image normalisation is applied using a local averaged image with filter length of 300 pixels, in order to reduce differences in particle image intensity distributions across the camera images. A 3×3 Gaussian smoothing and a sharpening filter are also applied to the image.

During the initialisation of the STB analysis, a triangulation step using iterative particle reconstruction is initiated to determine the particle positions in the 3D space, followed by a 'shaking' step where the 3D positions are adjusted in small steps (0.1 voxel) in order to find the best possible match with the particle projections in the different camera images (Wieneke, 2013). During this step, the use of the OTF ensures that the optical properties of the experimental set-up are taken into consideration and allow for an accurate determination of the 3D particle positions. Furthermore, the use of time-resolved data allows the STB algorithm to use previous time steps (after an initialisation phase) in order to predict the new particle position at the current time-step and therefore speeding up the computation by removing part of the effort in the triangulation process. The initialisation phase consists of four time-steps, during which the triangulation using iterative particle reconstruction is performed as described above, the obtained particle tracks are used to create a second order polynomial fit and extrapolated to the following time-step, providing a prediction of the new particle position. This new predicted position is also 'shaken' in order to maximise the match with the projected 2D particle images on the individual camera frames.

4 EXAMPLE OF APPLICATION

In this section, two example of results are presented to demonstrate this measurement technique for tidal turbine hydrodynamics research. Specifically, we will focus on the formation of the tip vortices and their evolution up to one diameter downstream of the turbine.

4.1 Tip Vortex formation

Figure 3 shows the formation of the tip vortex from the blade, which, at this time step, is approx. pointing upwards towards the free surface. The second tip vortex on the right hand side is a slide of the first helicoidal ring of the wake.

This figure is achieved by combining together two VOIs, shifted by 150 mm in the streamwise direction, resulting in 50% overlap. For each VOI, we recorded 570 images within 2 seconds, which allowed observing 10 blades passing through the volume.

The two VOIs were recorded at different times. Hence, the measurements were synchronised by matching the instantaneous position of the vortex core in both volumes. The velocity field of the two

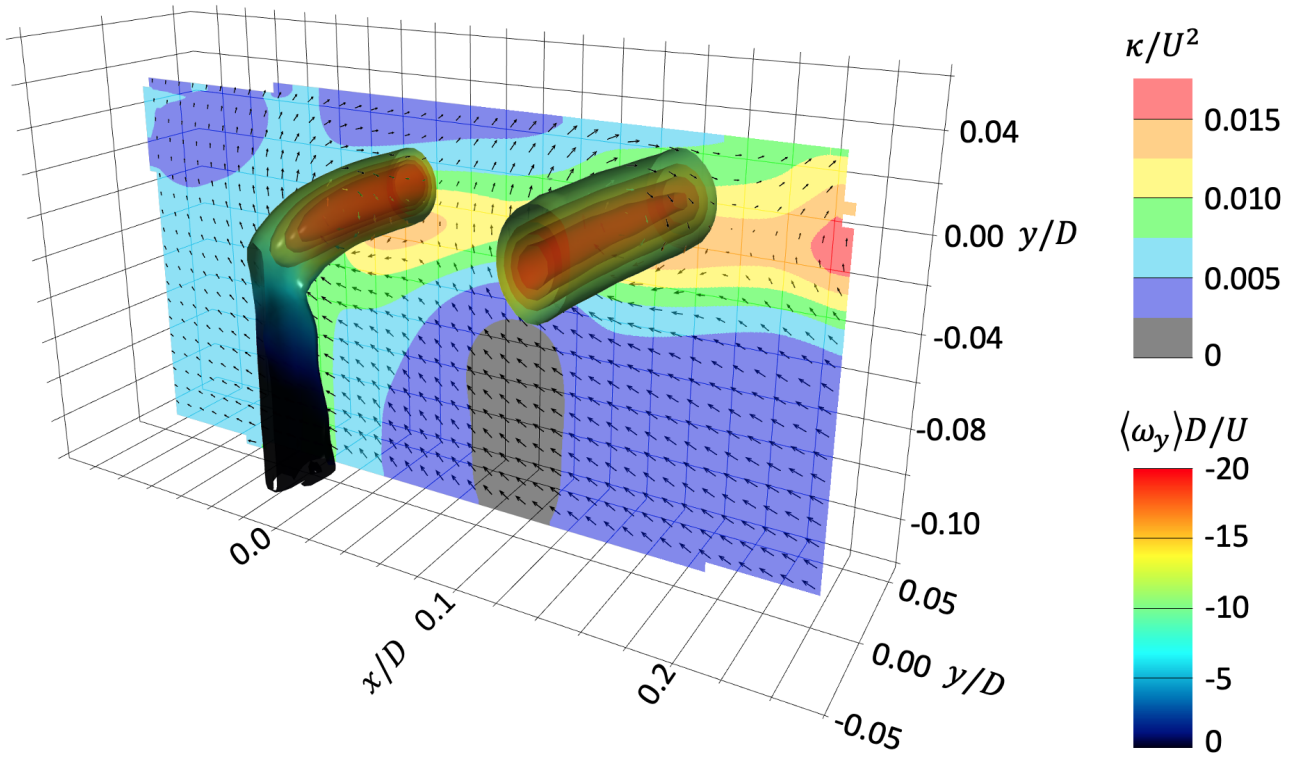

Figure 3. Vortex generation from the tip of the blade and a slide of the tip vortex formed one period of revolution before the current time frame. The coordinate system is centred at the tip of the blade, which is approx. vertical and pointing upwards. Time-averaged velocity vectors, as observed by an observer travelling downstream with the vortex convection velocity are plotted on the $y = 0$ plane (only every second vector is plotted). The plane is coloured by the turbulent kinetic energy κ. Tip vortices are identified by isosurface of shear strength $\langle\lambda_2\rangle$ of the phase-averaged flow velocity $\langle\boldsymbol{u}\rangle$. Isosurfaces are coloured by the phase-averaged y-component of the vorticity vector $\langle\omega_y\rangle$. All quantities are nondimensionalised with the rotor diameter D and the free stream velocity U.

measurements combined, $\boldsymbol{u} = (u, v, w)$, was used to compute the turbulent kinetic energy κ, which is plotted on the plane $y = 0$ in Fig. 3.

The velocity field is then binned to a regular grid, with bins of $96 \times 96 \times 96$ voxels, with an overlap of 83.3%. This resulted in a grid step size of 16 pixels in each direction, equivalent to 5.4 mm. The binned velocity field is then phased-averaged over ten blade passes, resulting in a time series of 57 time steps. The phased-averaged velocity field $\langle \boldsymbol{u} \rangle$ is used to compute the isosurfaces of swirling strength $\langle \lambda_2 \rangle$ that identify the tip vortices in Fig. 3, and the y-component of the vorticity $\langle \omega_y \rangle$ by which the isosurfaces are coloured.

The mean streamwise convection velocity of the tip vortices was found to be $U_v = 0.828U = 0.717$ m s^{-1}. The velocity field $\langle \boldsymbol{u} \rangle - U_v$ seen by an observer travelling with the tip vortices, is showed by the velocity vectors on the plane $y = 0$ in Fig. 3.

The $\langle \boldsymbol{u} \rangle - U_v$ velocity field reveals how the velocity field is mostly governed by the induced velocity of the tip vortices. The wake expansion observed in Fig. 3, such that the tip vortex on the right hand side is higher than that being formed, is also the result of the self-induced velocity of the tip vortices. Each tip vortex experiences a positive and a negative induced vertical velocity due to the vortices downstream and upstream, respectively. The most upstream vortices have more vortices downstream than upstream, resulting in a net positive vertical velocity. It is also noted that the tip vortices convect near the middle of the time-averaged shear layer, indicated by the maximum κ in Fig. 3. This figure clearly shows how the potential-like tangential velocity around the tip vortices, although it significantly contributes to the budget of turbulent kinetic energy, does not enhance mixing as if it was a chaotic turbulent fluctuation. A result already statistically demonstrated by Lignarolo *et al.* (2015) using a triple decomposition of the turbulent flow fields. For this reason, closure models based on turbulent viscosity overpredict mixing and wake recovery immediately downstream of the rotor.

4.2 Near Wake

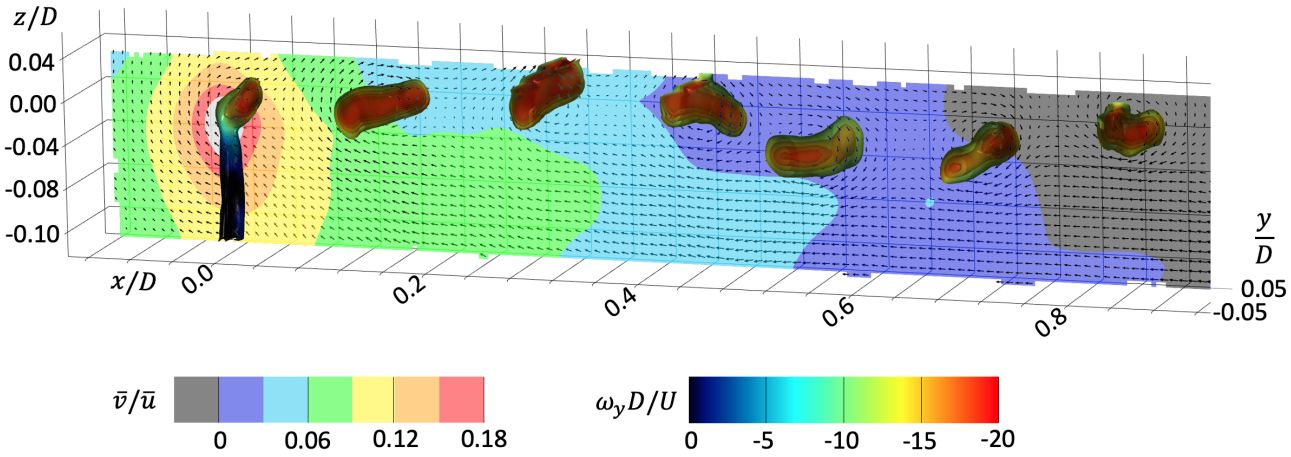

Figure 4. A vertical slide of the tip vortices within the first turbine diameter length of the wake at the same time step and with the same reference system as in Fig. 3. Tip vortices are identified by isosurface of λ_2 coloured by ω_y, both computed from the instantaneous (non phase-averaged) flow field. Time-averaged velocity vectors, as observed by an observer ravelling downstream at the vortex convection velocity U_v are plotted on the $y = 0$ plane (only every second vector is plotted). The plane is coloured by the ratio of the vertical ($\bar{v}$) and streamwise ($\bar{u}$) time-averaged velocities. All quantities are nondimensionalised with the rotor diameter D and the free stream velocity U.

Further 5 VOIs were measured, by translating downstream the MiniShaker and the LED units by 200 mm steps. This resulted in an extended measurement volume of approximately 1400 mm $\times$ 220 mm $\times$ 140 mm.

Figure 4 shows the near wake up to $0.9D$ downstream. Similarly to §4.1, the measurements were synchronised by matching the instantaneous position of the vortex core in the overlapping regions of the VOIs. The velocity field of the seven combined VOIs included 2500 time steps. The flow field of one of these time steps, when the blade is verical and pointing upwards, was used to compute the isosurfaces of λ_2 and the contours of ω_y by which the isosurfaces are coloured. It is noted that these isosurfaces are not as smooth as those in Fig. 3 because not phase-averaged. The 2500 flow fields were used also to compute the mean streamwise ($\bar{u}$) and vertical ($\bar{v}$) velocity components. Contours of the $\bar{v}/\bar{u}$ are plotted on the plane $y = 0$ in Fig. 3.

It is noted that $\bar{v}/\bar{u}$ is the arctangent of the direction of the in-plane mean velocity. Hence, by observing the contours of $\bar{v}/\bar{u}$, we can infer how the wake expands upto about $0.8D$ downstream of the turbine. This is when the vorticity of the extra vortices downstream becomes negligible and thus the net vertical induced velocity vanishes.

It is also noted that the streamwise distance between the tip vortices is higher for the first four vortices. This suggests that vortex pairing begins with the 5th tip vortex at approx. $0.5D$. Vortex pairing is the vortex interaction that precedes leapfrogging and then vortex breakdown (Okulov & Sorensen, 2004; Sørensen, 2011; Lignarolo *et al.*, 2015).

5 DISCUSSION AND CONCLUSIONS

This paper presented an underwater Lagrangian particle tracking velocimetry based on eye-safe LED illumination. Because it allows measuring relatively large volumes, it is particularly suited for large scale marine facilities where laser-based techniques such as stereo PIV is not possible for health and safety reasons. We demonstrated this technique by measuring the near wake behind a 1:15 scale tidal turbine with a diameter of 1.2 m in a 25-m-diameter, 2-m deep facility. We measured the flow field in 7 volumes 0.3 m long, 0.2 m wide and 0.1 m deep. Assuming periodic flow conditions, we combined these 7 volumes together with appropriate overlap to resolve the near wake within one diameter from the turbine. The flow field is measured with a time resolution of 3.9 ms (256 frames per seconds) and 5.4 mm.

To appreciate the richness of this data, it is noted that this is equivalent to 100 times the volume of investigation of a state-of-the-art stereo PIV, which have similar time and space resolution. In fact, stereo PIV typically allows measuring volumes that are similar in length and width, but only 1 mm in depth instead of 100 mm. The time resolution of stereo PIV is typically slightly lower (say 5.5 ms) whilst the space resolution could be slightly higher (say 2.5 mm).

Furthermore, because the system does not need to be re-calibrated once moved, different volumes can be easily combined together. For a periodic flow such as the wake behind a rotor, this allows achieving a time-resolved, phase-averaged flow field. The different volumes can be easily combined if flow measurements are synchronised with a measure of the angular position of the turbine. In this example, where the angular position was not known, we used the position of the vortex core in the overlap region between two adjacent volumes of interest.

Overall, the proposed methodology can enable a step change in the flow diagnostic capabilities of large scale marine facilities. The large volume and comparatively high time and space resolution could enable addressing key research questions on high-Reynolds-number flows and could provide valuable benchmark data for numerical model development and code validation.

ACKNOWLEDGEMENTS

The authors acknowledge the support from the UK Engineering and Physical Sciences Research Council for funding the FloWave Ocean Energy Research facility (Grant number EP/I02932X/1). The tidal turbine model was developed under the EPSRC-funded SuperGen UK Centre for Marine En-

ergy Research (EP/M014738/1) and the authors are grateful to the EPSRC and the grant's Principal Investigator, Dr Aristides Kiprakis, for kindly allowing its use for this investigation.

AUTHOR'S CONTRIBUTION

AN led the experimental investigation, with the assistance of TD and RG, and undertook the data processing. IMV coordinated the project and wrote the first draft of the manuscript.

References

Adcock, T A A, Draper, S, Willden, R H J & Vogel, C R 2021 The Fluid Mechanics of Tidal Stream Energy Conversion. *Annual Review of Fluid Mechanics* **53**, 287–310.

Adrian, Lara, Adrian, Ronald J & Westerweel, Jerry 2011 *Particle image velocimetry*. Cambridge university press.

Afgan, I., McNaughton, J., Rolfo, S., Apsley, D.D., Stallard, T. & Stansby, P. 2013 Turbulent flow and loading on a tidal stream turbine by LES and RANS. *International Journal of Heat and Fluid Flow* **43**, 96–108.

Ahmed, U, Apsley, D D, Afgan, I, Stallard, T & Stansby, P K 2017 Fluctuating loads on a tidal turbine due to velocity shear and turbulence : Comparison of CFD with field data. *Renewable Energy* **112**, 235–246.

Chamorro, L P, Hill, C, Morton, S, Ellis, C, Arndt, R E a & Sotiropoulos, F 2013 On the interaction between a turbulent open channel flow and an axial-flow turbine. *Journal of Fluid Mechanics* **716**, 658–670.

Chen, Yaling, Lin, Binliang, Lin, Jie & Wang, Shujie 2017 Experimental study of wake structure behind a horizontal axis tidal stream turbine. *Applied Energy* **196**, 82–96.

Day, A.H., Babarit, A, Fontaine, A, He, Y.-P., Kraskowski, M, Murai, M, Penesis, I, Salvatore, F & Shin, H.-K. 2015 Hydrodynamic modelling of marine renewable energy devices: A state of the art review. *Ocean Engineering* **108**, 46–69.

Draycott, S., Payne, G., Steynor, J., Nambiar, A., Sellar, B. & Venugopal, V. 2019 An experimental investigation into non-linear wave loading on horizontal axis tidal turbines. *Journal of Fluids and Structures* **84**, 199–217.

Elsinga, G. E., Scarano, F., Wieneke, B. & Van Oudheusden, B. W. 2006 Tomographic particle image velocimetry. *Experiments in Fluids* **41** (6), 933–947.

Felli, M., Camussi, R. & Di Felice, F. 2011 Mechanisms of evolution of the propeller wake in the transition and far fields. *Journal of Fluid Mechanics* **682**, 5–53.

Fontaine, Arnold A, Straka, William A, Meyer, Richard S & Jonson, Michael L 2014 A 1: 8.7 scale water tunnel verification & validation test of an axial flow water turbine. *Tech. Rep.*.

Gaurier, Benoît, Davies, Peter, Deuff, Albert & Germain, Grégory 2013 Flume tank characterization of marine current turbine blade behaviour under current and wave loading. *Renewable Energy* **59**, 1–12.

Gaurier, B., Druault, Ph, Ikhennicheu, M. & Germain, G. 2020 Experimental analysis of the shear flow effect on tidal turbine blade root force from three-dimensional mean flow reconstruction: Shear flow effect on tidal turbine blade. *Philosophical Transactions of the Royal Society A: Mathematical, Physical and Engineering Sciences* **378** (2178).

Lignarolo, L. E.M., Ragni, D., Scarano, F., Simão Ferreira, C. J. & Van Bussel, G. J.W. 2015 Tip-vortex instability and turbulent mixing in wind-turbine wakes. *Journal of Fluid Mechanics* **781**, 467–493.

Lloyd, Thomas P., Turnock, Stephen R. & Humphrey, Victor F. 2014 Assessing the influence of inflow turbulence on noise and performance of a tidal turbine using large eddy simulations. *Renewable Energy* **71**, 742–754.

Lust, Ethan, Luznik, Luksa, Flack, Karen & Barros, Julio 2015 Near Wake Flow Field Measurements of a Marine Current Turbine : Preliminary Results. *Oceans 2015* pp. 3–8.

Luznik, Luksa, Flack, Karen a., Lust, Ethan E. & Taylor, Katharin 2013 The effect of surface waves on the performance characteristics of a model tidal turbine. *Renewable Energy* **58**, 108–114.

Milne, I.A., Day, A.H., Sharma, R.N. & Flay, R.G.J. 2015 Blade loading on tidal turbines for uniform unsteady flow. *Renewable Energy* **77**, 338–350.

Noble, Donald R, Davey, Thomas A D, Smith, Helen C M, Kaklis, Panagiotis, Robinson, Adam & Bruce, Tom 2015 Spatial variation in currents generated in the FloWave Ocean Energy Research Facility. *Proceedings of the 11th European Wave and Tidal Energy Conference (EWTEC2015)* .

Noble, Donald R., Draycott, Samuel, Nambiar, Anup, Sellar, Brian G., Steynor, Jeffrey & Kiprakis, Aristides 2020 Experimental assessment of flow, performance, and loads for tidal turbines in a closely-spaced array. *Energies* **13** (8).

Nuernberg, M. & Tao, L. 2018 Experimental study of wake characteristics in tidal turbine arrays. *Renewable Energy* **127** (2018), 168–181.

Okulov, V. L. & Sorensen, J. N. 2004 Instability of a vortex wake behind wind turbines. *Doklady Physics* **49** (12), 772–777.

Olczak, A., Stallard, T., Feng, T. & Stansby, P. K. 2016 Comparison of a RANS blade element model for tidal turbine arrays with laboratory scale measurements of wake velocity and rotor thrust. *Journal of Fluids and Structures* **64**, 87–106.

Ouro, Pablo & Stoesser, Thorsten 2019 Impact of Environmental Turbulence on the Performance and Loadings of a Tidal Stream Turbine. *Flow, Turbulence and Combustion* **102** (3), 613–639.

Payne, Grégory S., Stallard, Tim & Martinez, Rodrigo 2017 Design and manufacture of a bed supported tidal turbine model for blade and shaft load measurement in turbulent flow and waves. *Renewable Energy* **107**, 312–326.

Raffel, M, Willert, C E, Wereley, S T, Kompenhaus, J, Scarano, F, Kähler, C J, Wereley, S T & Kompenhaus, J 2018 *Particle image velocimetry: A practical guide*, 3rd edn. Springer.

Roettig, Felix, Wennemar, Katharina, Hoyer, Katja, Beslac, Radomir, Hesseling, Christina, Beck, Tarek & Friedhoff, Benjamin 2019 Volumetric Flow Measurements in the Wake of a Ducted Propeller.

Schanz, Daniel, Gesemann, Sebastian & Schröder, Andreas 2016 Shake-The-Box: Lagrangian particle tracking at high particle image densities. *Experiments in Fluids* **57** (5), 1–27.

Schanz, Daniel, Huhn, Florian & Schröder, Andreas 2018 Large-Scale Volumetric Flow Measurement of a Thermal Plume Using Lagrangian Particle Tracking (Shake-The-Box).

Shi, Weichao, Atlar, Mehmet & Norman, Rosemary 2017 Detailed flow measurement of the field around tidal turbines with and without biomimetic leading-edge tubercles. *Renewable Energy* **111**, 688–707.

Sørensen, Jens Nørkær 2011 Aerodynamic Aspects of Wind Energy Conversion. *Annual Review of Fluid Mechanics* **43**, 427–448.

Stallard, T, Collings, R, Feng, T & Whelan, J 2013 Interactions betweem tidal turbine wakes: Experimental study of a group of 3-bladed rotors. *Philosophical Transactions of the Royal Society of London: A* **371** (1985), 1471–2962.

Stallard, T., Feng, T. & Stansby, P. K. 2015 Experimental study of the mean wake of a tidal stream rotor in a shallow turbulent flow. *Journal of Fluids and Structures* **54**, 235–246.

Tedds, S. C., Owen, I. & Poole, R. J. 2014 Near-wake characteristics of a model horizontal axis tidal stream turbine. *Renewable Energy* **63**, 222–235.

Usherwood, James R., Cheney, Jorn A., Song, Jialei, Windsor, Shane P., Stevenson, Jonathan P.J., Dierksheide, Uwe, Nila, Alex & Bomphrey, Richard J. 2020 High aerodynamic lift from the tail reduces drag in gliding raptors. *Journal of Experimental Biology* **223** (3).

Wieneke, B. 2008 Volume self-calibration for 3D particle image velocimetry. *Experiments in Fluids* **45** (4), 549–556.

Wieneke, Bernhard 2013 Iterative reconstruction of volumetric particle distribution. *Measurement Science and Technology* **24** (2).